Article

Seismic Signatures and Site Characterization of An Intermittent Stream in Dry and Flood Conditions: An Implication for Soil Losses and Landslide Triggering

Yawar Hussain[1*], Helena Seivane[2], Gao Qiangshan[3], Susanne Maciel[4], Omar Hamza[5], Rogério Uagoda[6], Welitom Borges[7]

[1]Georisk & Environment, Department of Geology, University of Liege, Liege, 4000, Belgium
[2]Andalusian Institute of Geophysics and Earthquake Disaster Prevention, University of Granada, Granada, Spain
[3]State Key Laboratory of Space Weather, National Space Science Center, Chinese Academy of Sciences, Beijing, China
[4] Planaltina Campus, University of Brasília, Brasília, Brazil
[5]School of Built and Natural Environment, University of Derby, Derby, UK
[6]Department of Geography, University of Brasilia, Brasilia, Brazil
[7]Institute of Geosciences, University of Brasilia, Brasilia, Brazil
* Correspondence: yhussain@uliege.be

Abstract

Identifying ambient noise-based (ANb) signatures of streams can help in the estimation of their erosive potential (EP) that promotes reverie landslides and soil losses in the fluvial valleys. This is particularly imperative on flooding or rainy days, leading to stronger erosion-prone conditions (colluvium and boulders) of the valley beds inferred from georadar attribute analysis. Developing such research direction can benefit the local communities, as is the case with the Cerrado region of Brazil, where these phenomena have high destructive potential with social, economic, and climatic implications. For the present study, a seasonal stream in the Federal District of Brazil was investigated by ANb monitoring supported by Ground Penetration Radar (GPR) for site characterization. The ANb monitoring was conducted (at a safe distance) with a seismometer over several durations of dry and rainy conditions. The power spectral density (PSDs) was computed as a function of several variables, including weather conditions (rainfall, wind speed, and pressure), time-frequency spectrograms, and ambient noise displacement root mean square (RMS). This analysis also considered the single station horizontal-to-vertical spectral ratio (HVSR), where rain, wind, pressure, river flow and anthropogenic signatures were evident (at selective frequency ranges). Multi-peaks that emerged on the HVSR curve were further analyzed to identify amplitude and frequency changes, and the three peaks shift on average to a lower position during the rainy period. The GPR amplitude and waveform variation features were attributed to the stratigraphy (i.e., the boundary between valid and invalid regions and coherence value) of the floodplain and regions susceptible to erosion (erosion-prone lithological spots). This approach provides the basis for non-destructive monitoring tools enabling the detection of 'seismic signatures' and weak spots of the fluvial channels for improving environmental management.

Keywords: weak spots; spectral analysis; ambient noise RMS; georadar attributes

1 Introduction

In recent years, floods and debris flow worldwide have increased riverbank and soil erosion and landslides, impacting the downstream communities and causing severe losses in lives, properties, and land functionality (Somos-Valenzuela et al. 2015; Zhang et al. 2022). Usually, local and small-scale erosions might not seem like serious instability problems. Still, in the long-term and extreme flood events, this situation often develops into landslides on riverbanks. It may also induce several issues, such as river blockage, a shift of river channel position, or flooding from rising riverbeds

 doi:10.20944/preprints202209.0447.v2

(Gu et al. 2020). Consequently, it may lead to the collapse of roads and bridges built along the river network (Chmiel et al. 2022).

With the effect of climate change, intermittent and ephemeral systems are expected to become increasingly common globally. However, these systems are understudied compared to perennial stream flows. These are of particular concern as they present a unique connection point at the terrestrial-aquatic interface, promoting soil erosion and landslide triggering. Moreover, complex spatial and temporal variations in hydrologic connectivity in non-perennial systems often require a unique interdisciplinary approach to advance the understanding of their function and response to global change. Therefore, monitoring riverbanks and erosive potential (EP) at an early stage is essential to inform the hazard evaluation and improve the risk management of erosion and landslide in such regions.

Fundamentally, EP is a function of various influencing factors, such as rainfall intensity (Rindraharisaona et al. 2022) and the nature of sediment transport and incision in the catchment area (Lawler 1993). In addition, the local site condition can play a vital role in this process. This condition may include the types and properties of soil, such as density (compaction), porosity, and permeability, and any variation in these properties that may represent potential shear plans (Hamza et al. 2020), soil thickness, the topography of bedrock, and the presence of rock fragments (Hussain et al. 2022). The EP assessment has a wide range of applications in landscape evolution, soil erosion, landslide, ecology, water quality, land use management, and civil and river engineering like dams and recreational reservoir silting (Giménez et al.; David et al. 2010; Oeurng et al. 2010; Graf et al. 2010; Araujo et al. 2012; Schmandt et al. 2013; Chao et al. 2015; Lai et al. 2018; Marchetti et al. 2019).

The accurate monitoring and prediction of EP of a river are challenging tasks. For such tasks, there are currently several adopted techniques, including (i) the stream hydrophones or geophones (Turowski et al. 2011), (ii) the identification of particles with a tracer or radiofrequency (Schneider et al. 2014), and (iii) calculation via empirical relationships calibrated in the laboratory (Wilcock and Crowe 2003). However, these techniques can be logistically challenging, particularly in significant flooding events, so their application becomes cost-prohibitive (Roth et al. 2016).

As river activity and site conditions of the valleys are coupled with physical properties, including the ambient noise and electromagnetic wavefields, among others, hence can be valuable sources for monitoring (time-variant) and characterization (time-invariant) using geophysical techniques. Thus, with the growing demands for remote monitoring of these signals from outside the river channel, geophysical methods are increasingly adopted for monitoring work.

For this remote monitoring of river flow, two types of seismic-based geophysical techniques are broadly emerging, where the generated seismic-based (GSb) and ambient noise-based (ANb) activities are measured. The seismic signals emitted by river dynamics can be monitored by non-invasive, cost-effective, long-term, and continuous methods with broad applications (Schmandt et al. 2013; Gimbert et al. 2014). Significant efforts have been made to quantify the spectral signature of bedload transportation water; however, it has been found that seismic power at low frequency is primarily generated by water discharges rather than bedload transportation (Burtin et al. 2008; Schmandt et al. 2013; Barrière et al. 2015). A theoretical model of PSD was calculated from the Rayleigh waves generated by saltating the bedload particles (Tsai et al. 2012). Another seismic activity produced by the turbulent river flow-based theoretical model was proposed by (Gimbert et al. 2014); it contributes to SPD variations in response to the seasonal hysteresis magnitude variations and has been reported in many other studies (e.g., Burtin et al. 2008, 2011; Schmandt et al. 2013; Chao et al. 2015; Barrière et al. 2015). These findings support the use of seismic for the high-resolution monitoring of river bedload and other flow attributes (Roth et al. 2016). From the previous studies, it can be concluded that for larger fluvial systems, high frequency (> 15 Hz) power excitation is created by high levels of bedload transportation (Schmandt et al. 2013; Roth et al. 2016;

Preprints (www.preprints.org) | NOT PEER-REVIEWED | Posted: 16 November 2022 doi:10.20944/preprints202209.0447.v2

Anthony et al. 2018). In contrast, turbulent flow and discharge modulate lower frequency seismic power (between ~1-10 Hz) (Burtin et al. 2011; Schmandt et al. 2013; Bartholomaus et al. 2015; Anthony et al. 2018).

Contrary, in ANb, the river-sponsored variations in the ambient noise wavefield are induced because of the impacts of the bedload on the riverbed and banks, flow noise generated by the water turbulence, and in response to the acoustic waves generated by the interaction of water and atmosphere (Díaz et al. 2014; Chao et al. 2015; Bakker et al. 2020; Lagarde et al. 2021). Monitoring such river-generated noise is consistently reported in hydrologic studies (Díaz et al. 2014). ANb monitoring techniques can provide high temporal and spatial resolutions of the landscapes, and their demands are increasing in bedload monitoring because of their low cost and non-invasiveness (Roth et al. 2016). In the past, an increasing number of contributions have been developed using the variations in ambient noise as the basis of the study of the river flow system (Burtin et al. 2008; Goodling et al. 2018; Anthony et al. 2018; Smith and Tape 2019; P.C and Sawazaki 2021). It was also found that the river discharge vs noise power followed a seasonal hysteresis trend consistent with the regional sediment transport rates in the river (Gabet et al. 2008).

To better decipher the EP of a river, particularly to better monitor the damage potential during floods episodes, the characterization of river beds and valleys can be achieved by GPR application (Arcone et al. 1998; Szuch et al. 2006; Weihermüller et al. 2007; Chalikakis et al. 2011; Fabregat et al. 2019). Overall, soil compaction affects soil dielectric constant and GPR EM signals, as reported in previous studies (Wang et al. 2016).

As in the case of the Cerrado region of Brazil, especially in active geomorphological valleys such as *Ribeirão Contagem valley,* erosion by water is a crucial soil threat and a significant cause of riverside landslides (Hussain et al. 2017; Gomes et al. 2019; Fonseca et al. 2022; Cunha et al. 2022). The present study considered an intermittent stream for the analysis that generates small seismic energies related to the sediments and water flows during rainy days in the Federal District of Brazil for the first time. In the first stage, an attempt has been made for the non-invasive detection of weak spots, susceptible to erosion and landslide, and subsurface layering based on geology (soil, boulder, bedrock) and degree of compaction (less compacted, more susceptible to erosion) by GPR attribute analysis. Afterwards, the contribution is focused on analyzing how the variations of water discharge in a small river can be observed and monitored using ambient noise analysis. We applied a new monitoring technique that calculates the displacement RMS amplitudes, PSD, spectrograms, and HVSR curves of ambient noise recorded during dry and rainy days. Additionally, HVSR peak attributes (i.e., amplitude and frequency) and their changes in relation to different meteorological factors are included in the analysis. The study offers insight into the approach applied, which can benefit the broader scientific community involved in the environment and geohazard management under future climate change extreme scenarios.

2 Material and Method

2.1 Study site description

The Ribeirão Contagem watershed is extended over 146 km^2 in the northern part of the Federal District of Brazil in the Sobradinho administrative unit (Figure 1). The study area has a translational landslide whose dynamism is controlled by river erosion (Hussain et al. 2019a). There are alluvial and colluvial materials weathered from the bedrock of the Paranoá group, though bedrock exposures within the channel itself are rare. Most of the Contagem catchment is located on a large erosion complex, where highly active hill slopes supply the channel during summer rainfalls (Ferreira and Uagoda 2015). The Maranhão river is the main tributary of the watershed that flows in the north and northeast directions. The drainage and channel densities of the watershed are 5.7 and 32.9 channels/km^2, respectively. The climate in the area is semi-humid tropical, with a rainy summer and dry winter. The mean annual precipitation in the area is 1,442.5 mm.

Preprints (www.preprints.org) | NOT PEER-REVIEWED | Posted: 16 November 2022 doi:10.20944/preprints202209.0447.v2

The soil analysis included granulometry, and geotechnical tests were performed on the samples collected with an auger and from trenches (Ferreira and Uagoda 2015). As a result, six soils types are identified in the Contagem basin, including deep and reddish oxisols on the hilltops, shallow inceptisols on the hillslopes, and ultisols because of the presence of clayey carbonate-rich rocks on valleys and plinthic oxisols on the border of hilltops. The erodibility (K factor) is larger for plinthic oxisols than the oxisols and ultissols, having an average value of 0.005790 ton.ha.h.MJ-1.ha-1.mm-1 and 0.004490 ton.ha.h.MJ1.ha-1.mm-1, respectively. The clayey soils in steep hillslopes (from 20° upper to 35° in hills and valleys) can control various linear erosional features such as gullies and landslides, e.g., creeps and translational, rotational movements. A significant proportion of these erosive features is found in inceptsoil in clay-rich rocks. About 63% of these features occur in close proximity to the river (~20 m), highlighting the active role of hydrological processes in erosion (Ferreira and Uagoda 2015).

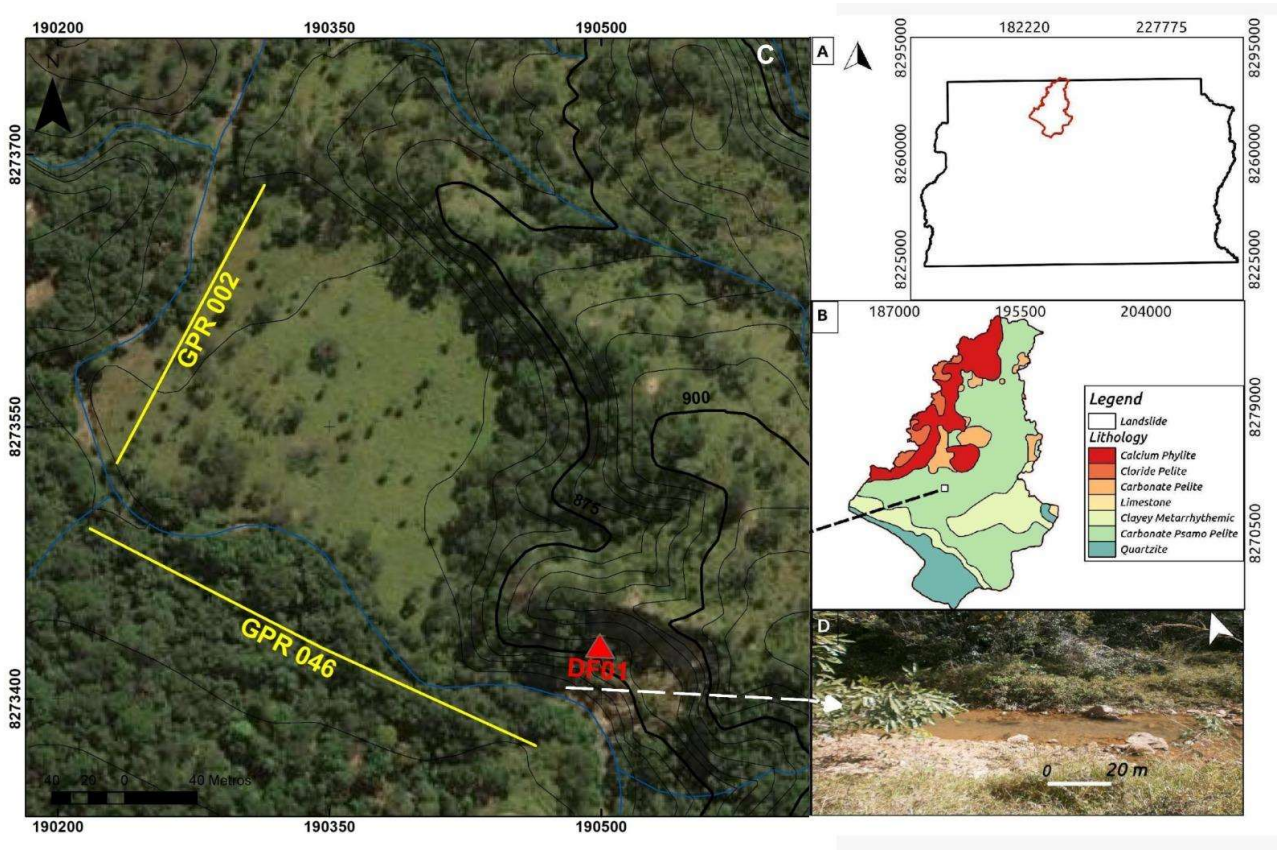

Figure 1. a) Geographic location of Ribeirão Contagem watershed on Federal District map, b) litho-technical units of the watershed c) red dashed ellipse is the Sobradinho landslide boundary and triangle is the position of seismometer (Hussain et al. 2019b) and D) the photograph of river floodplain in the dry season.

The Sobradinho Unit of Votorantim Cimentos Brazil is located in the Ribeirão Contagem Basin, where low-grade metamorphic sediments of the Paranoá and Canastra groups occur. The area is dominated by pelitic rocks such as gray slates and clayey metasiltites. The thickness of the unit varies between 120 m and 150 m, and the rocks that make up this unit are strongly influenced by the paleogeography of the bottom, marking the end of the deposition of the Paranoá Basin. Due to the composition of this unit, the primary minerals, when in contact with water or subjected to atmospheric conditions, are quickly weathered. The riverbank shows the connection between the colluvial-alluvial material and the alluvial material. The latter has a lateral continuity that varies between ~30 m and ~100 m long from the drainage bed (da

Preprints (www.preprints.org) | NOT PEER-REVIEWED | Posted: 16 November 2022 doi:10.20944/preprints202209.0447.v2

Silva Nunes et al. 2019). In the drainage bed, it was possible to observe that the finer-grained alluvial material (with well-selected grains, secondary minerals and low humidity) was superimposed on the colluvial material with poorly selected grains (varying from medium sand to gravel with decimetric boulders), composed of quartz with a high moisture content due to shallow water table. In general, the deposits in the Ribeirão Contagem channel are distributed as follows: soil masses moved by recent rotational landslides; river sediments deposited in recent river bars; sediments deposited in an alluvial fan; colluvial sediments; and alluvial sediments.

Figure 2. a) The former terraces eroding sites (b) photographs of various sizes of sediments from clay to pebbles and boulders in the riverbed, showing the transport capacity in river floods (c) the sediment sequence in terraces show clayey levels and on top with a clast supported layer on the base, showing events of high energy where recurrent (d) sites of undercutting of steep slopes inducing landslides by the river.

Ferreira and Uagoda 2015 proposed a classification for estimating EP based on hydrological units, slopes, and forms. Three classes were found in the Contagem basin as low, medium, and high EP. Concave hillslopes higher than 10° were classified as high potential due to subsurface flux and clayey material concentration. While on convex slopes, the critical to a movement was taken as 35°. The map showed the major proportion of known mass movements wherein high potential. So, the fluvial valleys and their steep hillslopes are dynamic areas composed of alluvium in the bottom, colluvium in the low and middle parts of the high slopes, shallow inceptsols in the elevated portion of the hillslopes, and oxisols in the hilltops. The concave hillslopes have a critical angle of up to 10°, being the most important trigger of rotational landslides on the border of deep valleys (Braga et al. 2018).

Preprints (www.preprints.org) | NOT PEER-REVIEWED | Posted: 16 November 2022 doi:10.20944/preprints202209.0447.v2

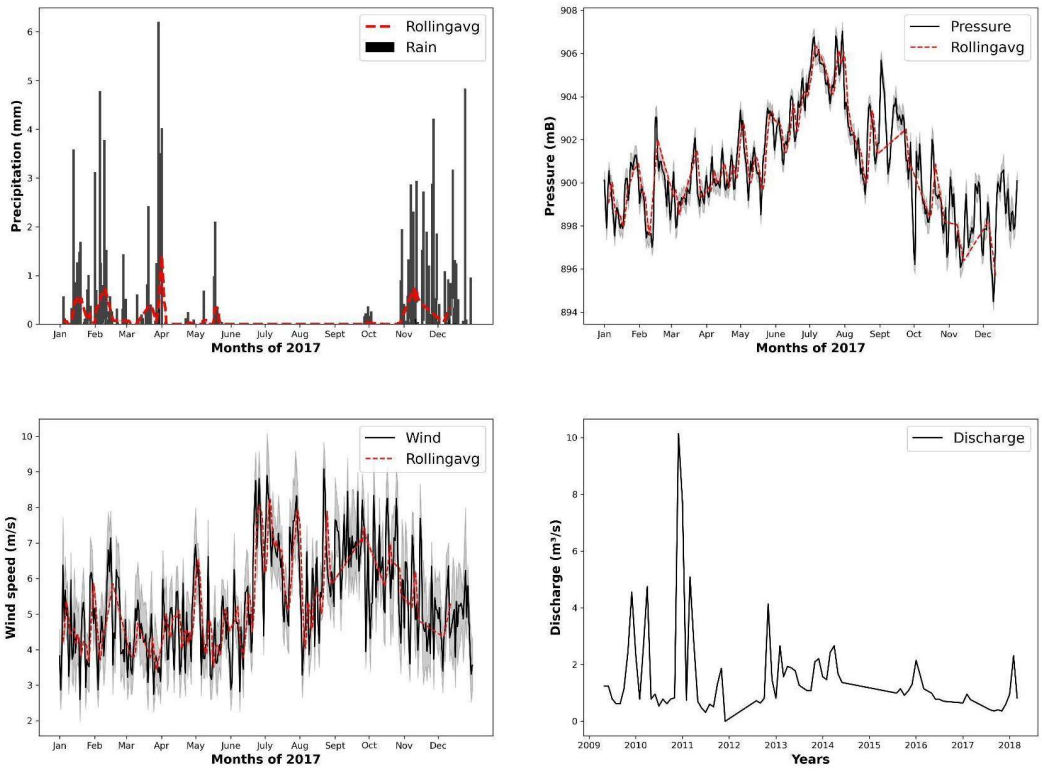

Figure 3 (a) Rainfall, (b) pressure, (c) wind speed and (d) river flow plots of the area.

2.2 Data Acquisition and Processing

2.2.1 Seismic Ambient Noise

For hydrodynamic analysis of the river, one Sorcel L-4A-3D short-period seismometer having a natural frequency response of 2 Hz was installed at the bank of the river at the '*Rua do Matto'* locality (Figure 1). The continuous data for the seasonal impact evaluation was divided into two acquisition campaigns (1) dry from Julian day 101 to 105 of 2017 and (2) rainy period from Julian day 344 to 350 of 2017. The records were performed in a continuous mode and at a sampling rate of 250 samples per second with a DAS-130 RefTEK data logger. Raw ambient noise record for the rainy days is presented in Figure 4.

The ambient noise wavefields of dry and rainy days were compared by applying spectral analysis of the ambient noise recorded two times, including power spectral density estimation, time-frequency analysis by spectrogram, and possible quantification effects on the site response by HVSR. After spectral analysis, the displacement RMS of ambient noise of two-time series was also calculated using a widely adopted approach (Lecocq et al. 2020). Details of this processing are provided below.

a) The fast Fourier transform (FFT) of each component is applied to check the response of fluvial mechanisms under the same geological conditions on the same station. This way, the signal's decomposition into a discrete spectrum is achieved. The waveform of dry and flooding conditions is selected, consisting of ground motion records of N-S, E-W and Z components. The steps include (i) subdivision of data into smaller windows of time length 50-60 s each with 10% overlap, (ii) each window is 5% cosine tapered and transformed into Fourier domain, and (iii) each spectrum smoothed

Preprints (www.preprints.org) | NOT PEER-REVIEWED | Posted: 16 November 2022 doi:10.20944/preprints202209.0447.v2

prior to the calculation of spectrum for a bandwidth coefficient 40, as the raw signal contained unusual spikes (Singh et al. 2019; Pandey et al. 2020).

b) The amplitude spectrum is obtained by applying a further transform to the FFT. Power is obtained as a square of the amplitude spectrum. PSDs are gathered by binning periods and powers. These power-period bins are normalized to obtain the probabilistic power spectral density (PPSD). The PSD and its aggregation provide ambient noise energy (power) variations, so the signal strength and distribution are a function of frequency (Díaz et al. 2014; Pandey et al. 2020). For the validation of spectral analysis, PSD is plotted as functions of rainfall, wind speed, and pressure from the nearby meteorological station. These data are useful in correlating the variation of amplitudes in seismic noise with the sudden changes brought by rainfall, wind speed and pressure. These meteorological data are divided into ranges, and the changes in PSD are observed accordingly.

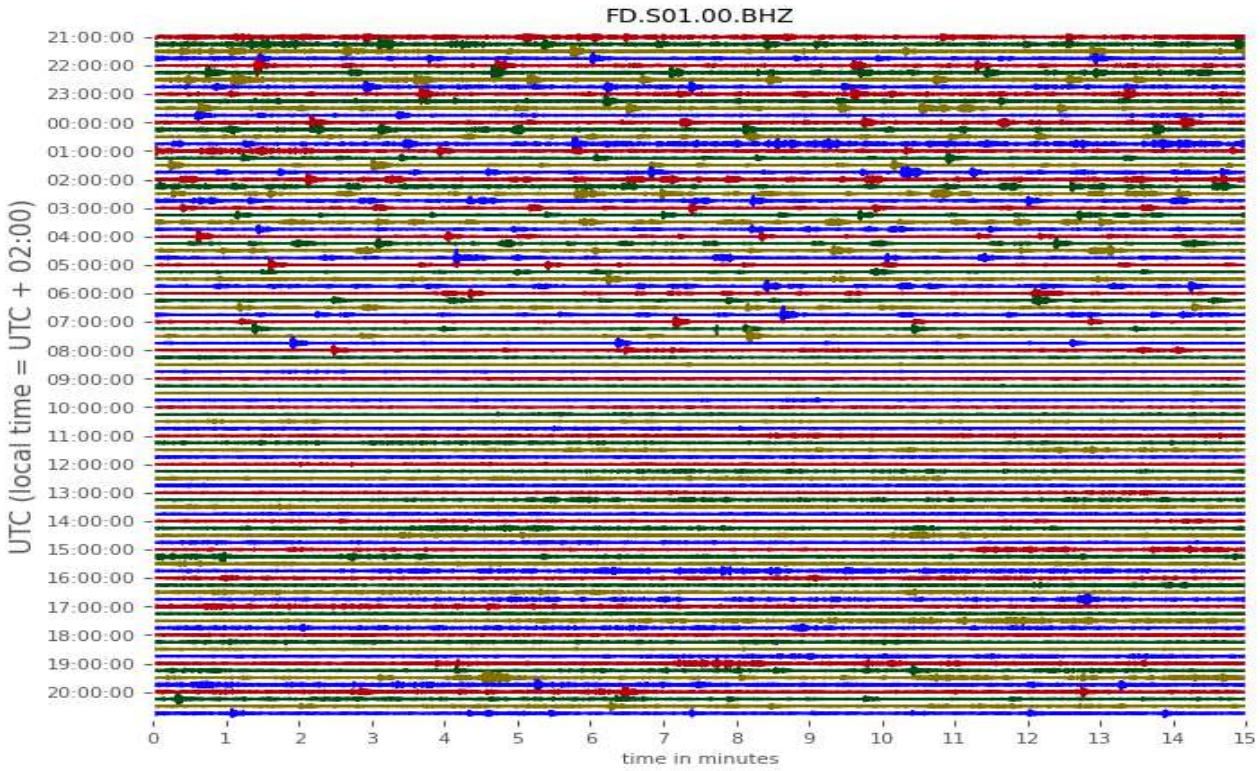

Figure 4. Seismograms recorded during rainy days. Periods of rainfall and river flow can be clearly seen in the plot.

c) As the seismic energy of a signal is proportional to the square of its amplitude; therefore, the root means square (RMS) analysis of a continuous record provides another way of highlighting the variations of seismic signals with time (Falanga et al. 2021). Displacement RMS of ambient noise records is calculated using a widely adopted methodology in "COVID Seismology" (Lecocq et al. 2020). It first calculates the PSD based on which the RMS displacement is derived. To access changes in RMS during hours of the day, clock plots are drawn at frequency bands of interest. In order to reduce the high energy ambient noise spikes, a time window of 0.1-7.0 hours is chosen. Similarly, to validate RMS results, change-point analysis (CPA), an approach for detecting the numerical value of change in two-time series, was adopted (Maciel et al. 2021). There are few case studies on the application of CPA in seismology as ambient noise interferometry (Sánchez-Pastor et al. 2018), landslide monitoring (Amorese et al. 2018), and seismic monitoring of COVID-19 (Maciel et al. 2021). An open-access python rupture library was used for the analysis (Truong et al. 2020). We choose Pruned Exact Linear Time (Pelt) algorithm, adopting a radial basis function model. It works on the assumption that the change point is unknown

Preprints (www.preprints.org) | NOT PEER-REVIEWED | Posted: 16 November 2022 doi:10.20944/preprints202209.0447.v2

and only a penalty parameter is required for the prediction. The choice of penalty is based on the iteration of a set of plenty values. We evaluated the precision and recall metrics for each segmentation for each value. The penalty value chosen was the one that optimized the precision-recall trade-off. This way, the change point is detected as a function of larger cost function intervals. In this study, we used the RBF cost function, a non-parametric approach based on a Gaussian kernel estimation. It can detect distribution changes rather than shifts in standard statistical measures, such as mean, mode, etc. A detailed explanation of the CPA approach and its application is explained by (Lykou et al. 2020; Maciel et al. 2021).

d) Time-frequency spectrograms are calculated using Obspy (a python library) inbuilt functions, which are expressed in units of energy as dB/(m^2/s^4) over different frequencies.

e) Changes in local site response can be an important contributor to soil erosion and landslide because detached soil blocks along the river bank have their natural period and are excited by the changes in Vs accordingly (Hussain et al. 2019a). Therefore, following (Goodling et al. 2018; Anthony et al. 2018), we applied the HVSR method (Nakamura 1989) to the three-component ambient noise records, which provide an ideal scenario for the estimation of site response due to changes in river flow. HVSR provides the response frequency of the loose sedimentary layer over the bedrock if there lies a considerable impedance contrast between them. Using this method, the natural period and the depth of the sedimentary layer are found using equation 1. The FFT of the vertical and horizontal ground motions is calculated after applying an energy normalization on each window following the diffuse approach for the HVSR methodology proposed by (Sánchez-Sesma et al. 2011). The spectra of both horizontal components are averaged following the vector summation described by (Albarello and Lunedei 2013) and divided by the spectral of the vertical component. In the end, results are smoothened by applying a smooth mean halfwidth 40, and results are plotted. More details about this process are provided elsewhere(Hussain et al. 2020a). Water infiltration and accumulation within unstable compartments may play a fundamental role in site stability. If the unstable compartment is susceptible to water retention, an increase in water content causes an increase in mass (M) and density (ρ). A decrease in both contact and bulk shear modulus (Gb) is simultaneously expected due to water seepage. A reduction in f1 and a negative dV/V are then expected. Lowering the water table and drying of the material generate the opposite effect (Colombero et al. 2021)

$$f_r = \frac{V_s}{4Z} \qquad (1)$$

where Z is the depth, fr is the natural frequency, and Vs is the shear wave velocity.

2.2.2 Ground Penetrating Radar

The dielectric constant of the soil and the degree of its compaction (bulk density/penetration resistance) are somehow related, as documented in the literature (Wang et al. 2016). This relationship can be utilized in fluvial seismology for the stratification of soil based on the degree of compaction, as loose or unconsolidated soil susceptible to erosion and possible related hazards such as bank erosion. This can also change the river dynamics by increasing the amount of sediment loads and water viscosity, which impacts the seismic (both ANb and ESb).

In this regard, two GPR profiles of 180 m and 360 m long were taken along with the riverbank during dry days using a georadar device GPR GSSI SIR 3000 (Geophysical Services Systems, Nashua, NH, USA), with 400 MHz antenna, control unity, and rugged survey car. The authors used the GPR attributes (i.e., coherence, average amplitude and average energy) for the detailed stratigraphy of the river floodplain as well as marks the degree of compaction (weak spots) of different superficial material types and their susceptibility is discussed in terms of their erodibility.

Preprints (www.preprints.org) | NOT PEER-REVIEWED | Posted: 16 November 2022 doi:10.20944/preprints202209.0447.v2

We used Reflex-win software, version 9.0.5, to do GPR data processing which included: i) static correction for the time zero setting; ii) The "energy decay" module was used to compensate for the signal decay; iii) applying the "background removal" module to suppress or remove the coherent noise or stationary wave noise; iv) 1D type bandpass frequency filtering for removal of high and low-frequency random noise, cutting intervals were set subjectively according to the frequency spectrum of some traces; v) The "running average" module was applied to do data smoothing, the average traces was set as three. After the 5th step, the average amplitude, average energy, and coherence attributes were extracted using the C Language we coded. Finally, the attributes were displayed by the Reflex-win software. The average amplitude attribute is extracted from traditional GPR data by calculating the average of all positive values within a fixed time window, while negative amplitudes are discarded.

In the next stage, the coherence attributes that measure waveform similarity of neighboring traces are calculated to interpret the features of the river floodplain. There are numerous applications of coherence in GPR signal processing (Gao et al. 2020), after its first use for seismic signals by (Bahorich and Farmer 1995) and first applied to GPR data by (Young et al. 1997). This method achieves coherence using a classical mutual correlation algorithm with 0 and 1 values, and results can be applied to determine valid and invalid signal regions along the GPR profile. Details are provided by (Gao et al. 2020). In the end, the coherence image is color scaled as white high and black low values. The boundary of these two signal classes (valid and invalid) is interpreted as a lithological boundary or maximum penetrating depth limit. Valid signals are reflection or echo waves that can be attributed to stratigraphy, while invalid signals are the random noise generated by the radar system itself (Jol 2008).

3 Overview of the findings

3.1 Spectral analysis of seismic ambient noise recordings

PSDs

As described earlier, the spectral analysis includes PSDs, and spectrograms of two ambient noise time series recorded during dry and flooding days. Additionally, the PSDs were plotted as a function of wind speed and rainfall. The possible imprints of rainfall on the ambient noise may include the noise because of rainfall drop, river discharge, and properties of sediment loads and check on the urban activities in hours of rain. The details of the findings and discussion are documented below.

PSD, as a function of rainfall, wind speed and pressure, are plotted to delineate the effects of these meteorological factors on the power of noise at different frequencies. The wind speed in the considered time is divided into two ranges (Figure 5a). Discharge effects on PSD are clearly seen on horizontal and vertical components. The PSD at low frequency is found unaffected by the wind speed at all considered ranges. However, both time series are directly related at high frequency i.e. PSD is higher at high wind speed and vice versa. Similarly, the rainfall amount during rainy days is divided into two ranges: 0.00-2.47 and 2.47-4.93 mm. Then PSD is plotted as a function of these ranges. It is interesting to note that, similar to wind speed, the high rainfall affects the ambient noise PSD at higher frequencies (Figure 6b). The spectral peaks remained the same on all PSD plots.

On PSD plots, the identification of river flow and its sediment loads are discussed in terms of variations in power and peak shifting (Wenner et al. 2019). These variations are assumed to be excited by the discharge and other related phenomena on rainy days. The changes can also be seen on low-frequency power; this may be associated with the flow considerations of flood-induced changes in the riverbanks' roughness (Roth et al. 2016). The peaks at higher frequencies in rainy days (Figure 5d) are associated with variations in the ambient noise wavefields brought by river-related

phenomena and effects of other resonant structures such as landslides, local stratigraphy and the other riverine resonant structures related to the deposition of sediments in the floodplain. It may be associated with the same propagating source in the river floods, as explained by (Piantini et al. 2021). Another possible explanation for these peaks could be the sudden destabilization of debris deposits on slopes and cliffs, which usually result from mass wasting (Chmiel et al. 2022).

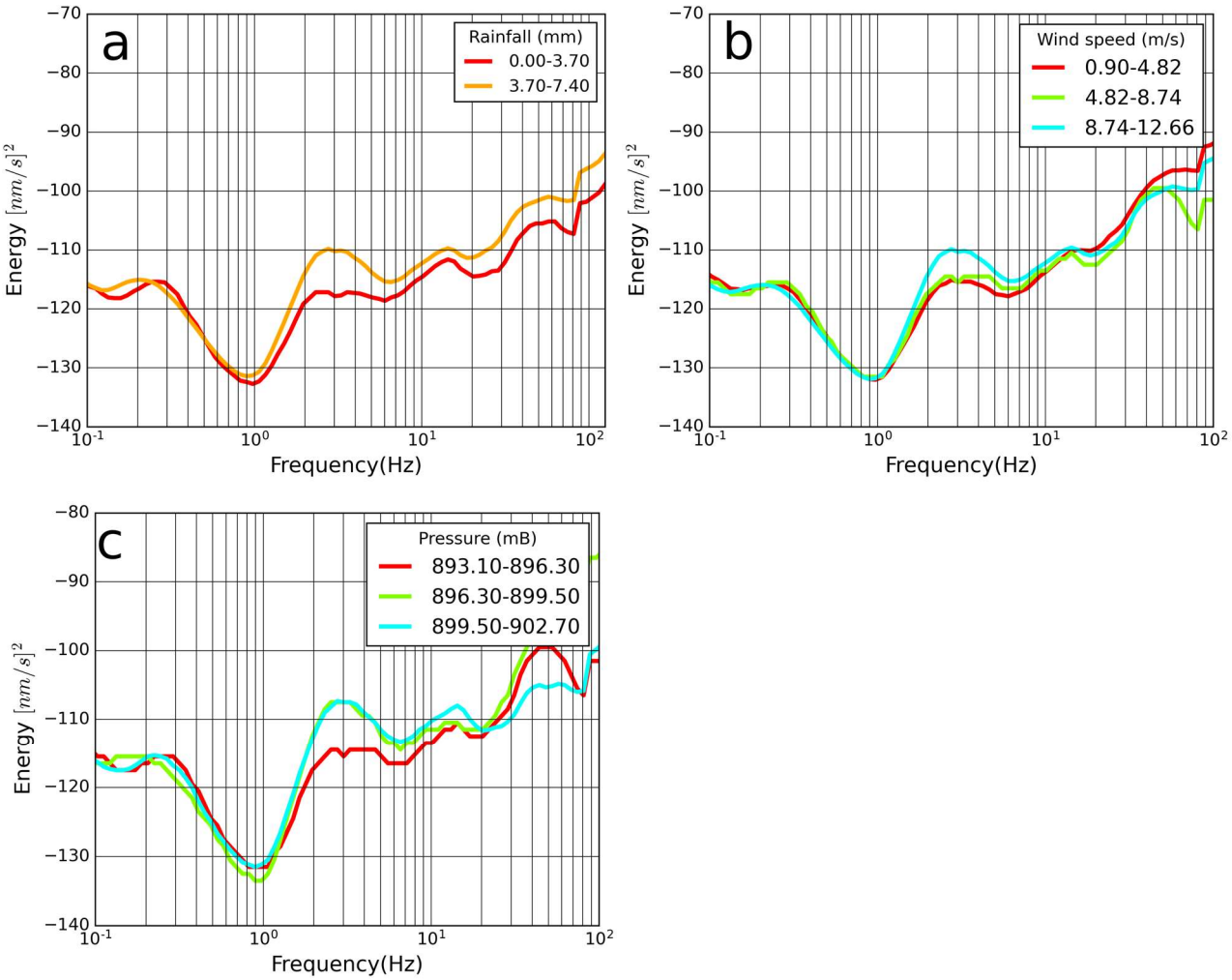

Figure 5. PSD as a function of a) rainfall, b) wind speed, and c) pressure during rainy days at the Z-component of the rainy record.

Figure 5a shows that with the increase in rainfall amount, there is an increase in PSD at a broad frequency range. Wind speed has different effects on the noise energy in rainy conditions; as the wind speed rises, there is an increase in PSD at a high frequency (2–20 Hz), while the lower frequency remains unaffected (Figure 5b). At a frequency range from 20-100 Hz, this trend does not hold. A similar trend of rising wind speed-increasing PSD during rainy days can be seen in Figure 5b. The fluvial effects on different frequency bands are documented in previous studies as 15–45 Hz (Schmandt et al. 2013), 5–15 Hz (Chao et al. 2015), 10-30 Hz (Schimmel et al. 2018) and ~0.1–45 Hz by (Anthony et al. 2018). The debris flow signature at the 5-10 Hz frequency band was observed by (Lai et al. 2018).

Spectograms

 doi:10.20944/preprints202209.0447.v2

The short-period spectrograms are shown in Figure 6, which present four different frequency bands (continuous or discontinuous). The spectrograms of two times show low-frequency ambient noise, query blats, and high-frequency noise. The significant energies induced by the river flow below 10 Hz and between 10-60 Hz can also be seen in Figure 6. These are combined effects of rainfall, river flow, and sediment loads. The sedimentary signals can be seen in Figure 6 as high-frequency events. The frequency band below 2 Hz is the instrumental noise; therefore, it was not possible to see the effects of high wind speed at low frequency. The other high-energy noise band is 2-12 Hz which can be seen on both dry and rainy plots to mark the effects of cultural noise. It also shows a diurnal pattern, another attribute that confirms the presence of cultural noise. The higher frequency band, 20–50 Hz, is only prominent on rainy days, showing river-related processes.

Interestingly, the quarry blast from the nearby mining can be observed on both spectrograms. The spectrograms of dry days don't show any energies at the frequency band where river influence emerged during rainy days. The quiet periods associated with lunch break hours (12-14) at frequencies below 10 Hz can be seen as small windows during rainy days. In literature, the river flow has been observed over different frequency ranges, which depend on the conditions of the river (discharge amount, roughness of river bed) and its site (soil conditions). (Polvi et al. 2020) reported stream flow and sediment transportation the frequency ranges as ~1–20 Hz and ~15–100 Hz, respectively. Very high energy peaks of the rainy spectrogram may be associated with the signatures of rain plus wind, as reported by (Rindraharisaona et al. 2022).

Preprints (www.preprints.org) | NOT PEER-REVIEWED | Posted: 16 November 2022 doi:10.20944/preprints202209.0447.v2

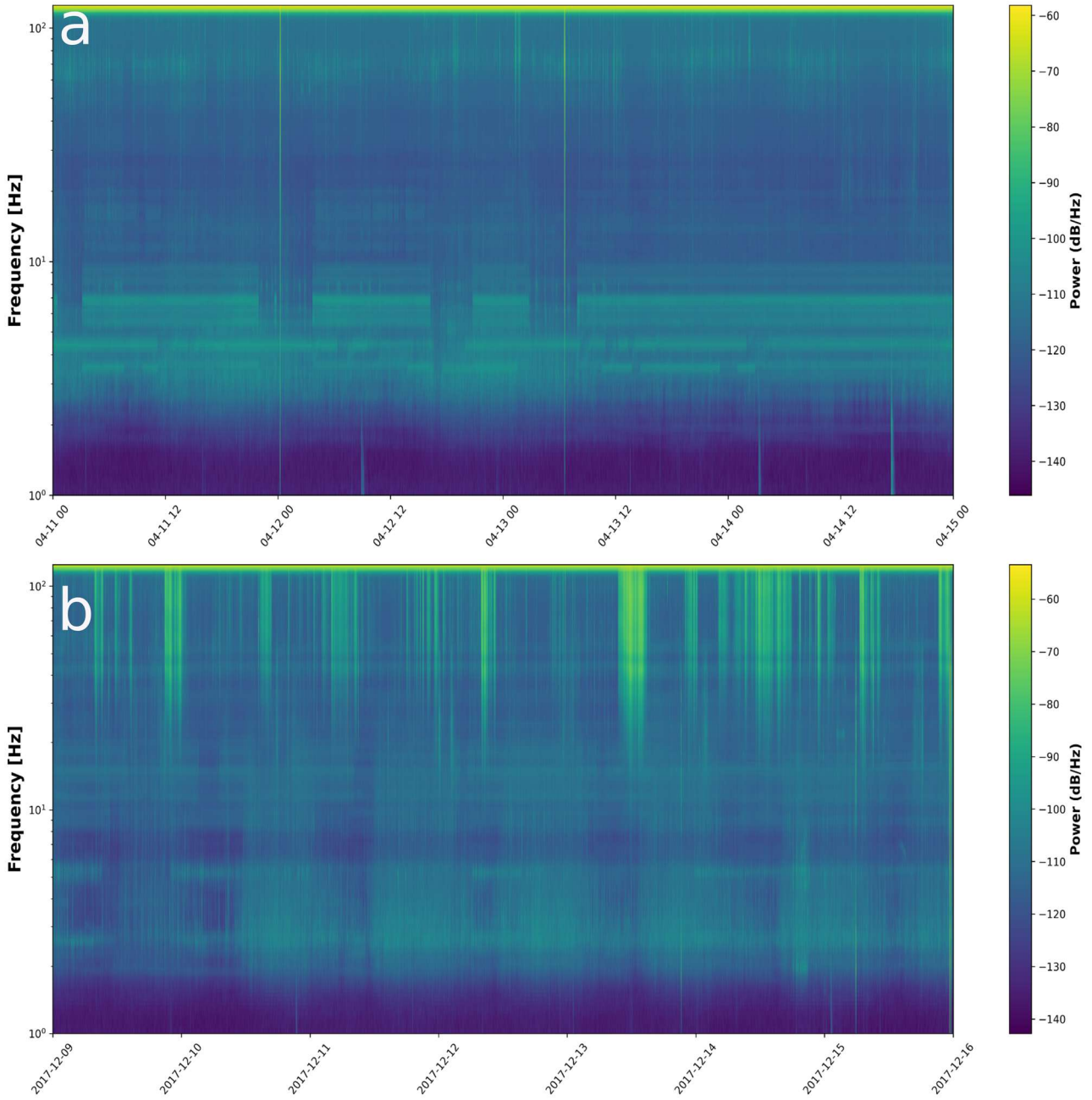

Figure 6. Spectrograms a) dry and b) rainy.

RMS amplitude and energy release

The ambient noise velocity RMS shows variations with hours of the day at different frequencies (2-5 Hz, 30-40 Hz, 50-70 Hz and 70-125 Hz) (Figure 7). It shows stability in ambient noise levels at low frequencies for both the considered time scales. At frequency bands of 30-40 Hz and 50-70 Hz, a decrease in RMS values is observed on rainy days, possibly associated with a break in anthropogenic activities because of rainfall. An increase in RMS is found at frequency ranges of 2-5 Hz and 70-125Hz. These are the possible frequency ranges where the combined effects (solid-fluid mixture) can be seen. However, the diurnal patterns can be seen in both series at higher frequencies. This may be associated with human activities and the influence of floods in the river at different frequencies; however, as the river is

Preprints (www.preprints.org) | NOT PEER-REVIEWED | Posted: 16 November 2022 doi:10.20944/preprints202209.0447.v2

small enough, the influences are less prominent on RMS plots. Under these limited data availability conditions, it is difficult to separate the urban noise and noise generated by the river.

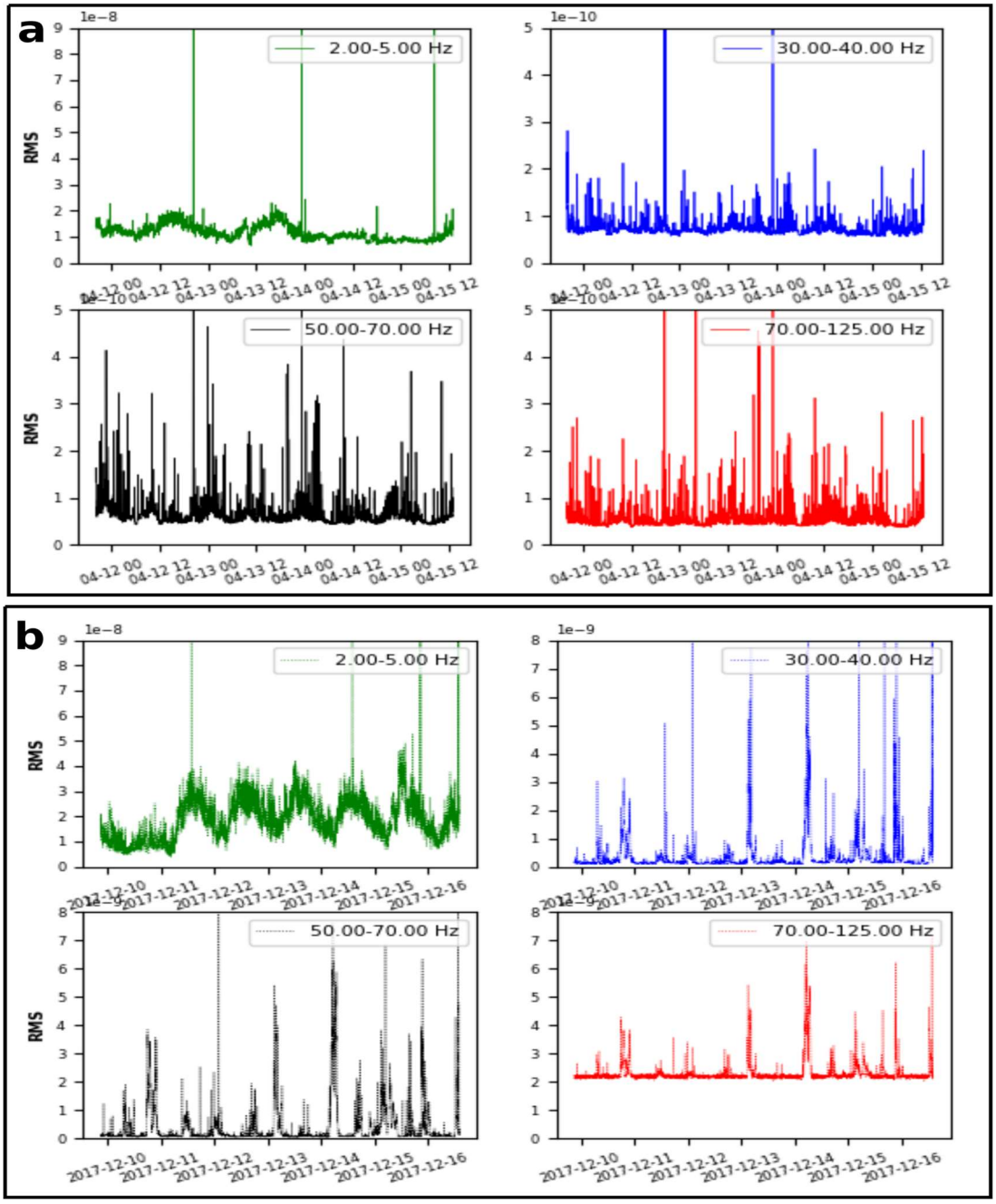

Figure 7. Displacement RMS amplitude of the ambient noise time-series average noise at 6h-16h hours of the day filtered at chosen frequency ranges (2-5 Hz, 30-40 Hz, 50-70 Hz and 70-125 Hz), a) dry and b) rainy days.

Change Point Analysis

Each changing point represents a change in the underlying distribution of the series. The correspondence between wind speed and seismic energy change points demonstrates that both phenomena are correlated somehow. In other words, there is an increase in ambient noise RMS with the wind speed and vice versa (Figure 8). The wind can have possible indirect effects by coupling with structures and vegetation on the ground as we buried the seismometer, so the direct impact of winds is negligible. These effects have also been highlighted in the literature. (Seivane et al. 2022), observed

Preprints (www.preprints.org) | NOT PEER-REVIEWED | Posted: 16 November 2022 doi:10.20944/preprints202209.0447.v2

the effects of wind speed on seismic records (HV curves), the ambient noise records and wind speed found well correlated in the Campo de Dalías basin in Spain. There is another study where the effects of windmills have been observed on ambient noise records (Saccorotti et al. 2011).

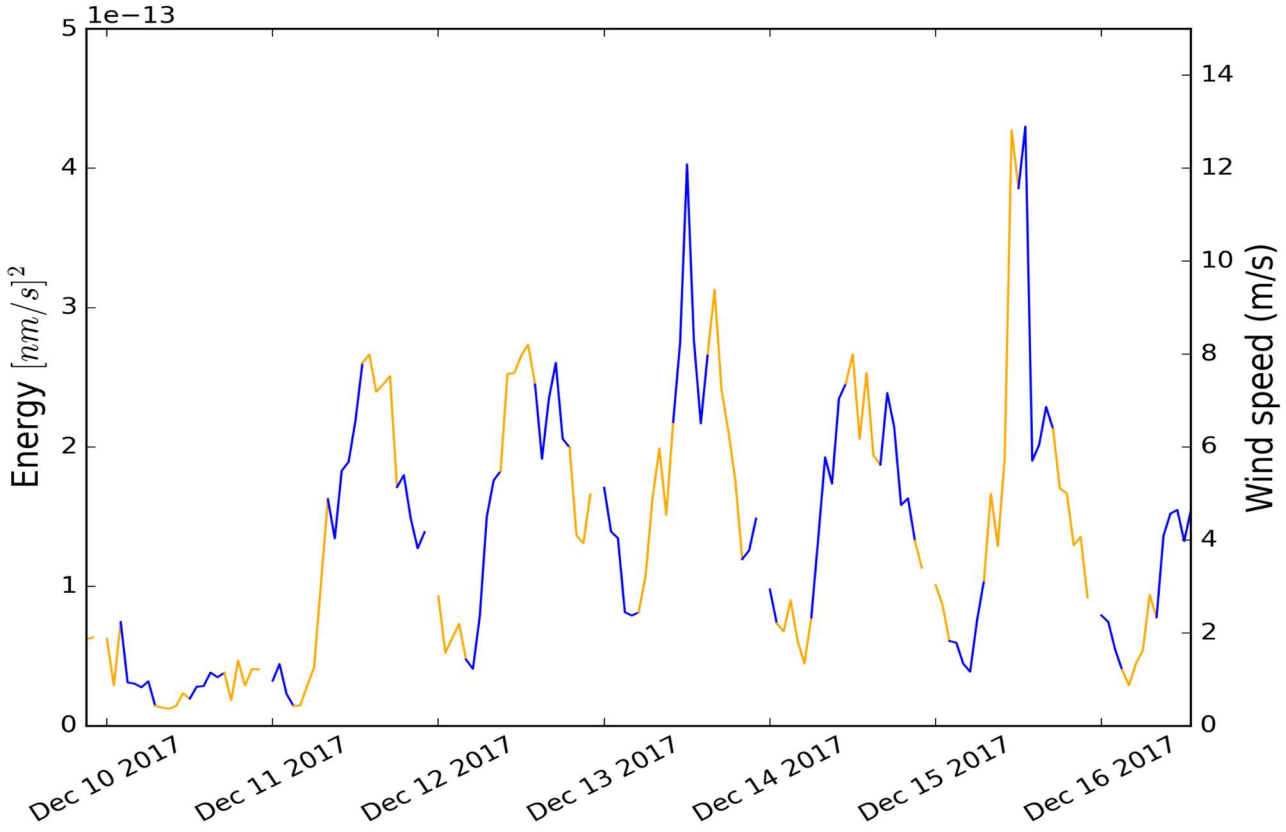

Figure 8. The change of color at each time series represents a change point automatically detected by a CPA algorithm.

HVSR curves

The HVSR curves obtained for the studied periods (rainy and dry) are characterized both by a condition of multiple-peak (Figure 9a). The fundamental HVSR peak identified by (Hussain et al. 2019a) as the contact between the low-velocity soft deposits and the Paranoá bedrock is also observed during both periods at 1.3 Hz. Moreover, the secondary peaks attributed to the landslide surface observed by (Hussain et al. 2019a) are also identified during the dry season at 4 and 9 Hz showing both significant HVSR amplitudes (SESAME 2004). This behavior agrees with the findings by (Hussain et al. 2019a) for these secondary peaks, which tend to decrease in amplitude or totally disappear during rainy days. On the other hand, the double peak found above 20 Hz is present in both periods (Figure 9b). It seems to slightly shift the frequency positions on average of each peak and vary the HVSR amplitude when comparing both periods.

In order to compare the differences between the two periods studied, Figure 10 gathers the HVSR variations, in terms of frequency and amplitude, for the two persistent peaks observed: the fundamental one at 1.3 Hz and the higher double peak between 20 and 100 Hz. During the rainy period, a wider variation is experienced in the two frequency bands, revealing a period of higher instability in the HVSR curves. Regarding frequency position, the three peaks shift on average to a lower position during the rainy period (Figure 10). Such observation agrees with the findings by (Stevens and James 2022), which revealed that the drops in f_0 coincide with sharp increases in water content. This is coherent with the overall soil moisture increase expected during heavy rainfalls in the study area. The daily variations show how a semi-diurnal

Preprints (www.preprints.org) | NOT PEER-REVIEWED | Posted: 16 November 2022 doi:10.20944/preprints202209.0447.v2

modulation on the HVSR amplitude exists for the highest secondary peaks, at 40 and 60 Hz, that is kept in both periods (Figure 11).

On the contrary, the amplitude variations of the fundamental peak have a daily modulation which loses clarity during the rainy period (Figure 11). While this daily modulation can be related to the well-known pattern of the cultural noise, the semi-diurnal behavior observed in the amplitude modulations of the highest peaks could show a tidal modulation likely induced by the river flow. This would support the hypothesis of the river origin behind these two peaks.

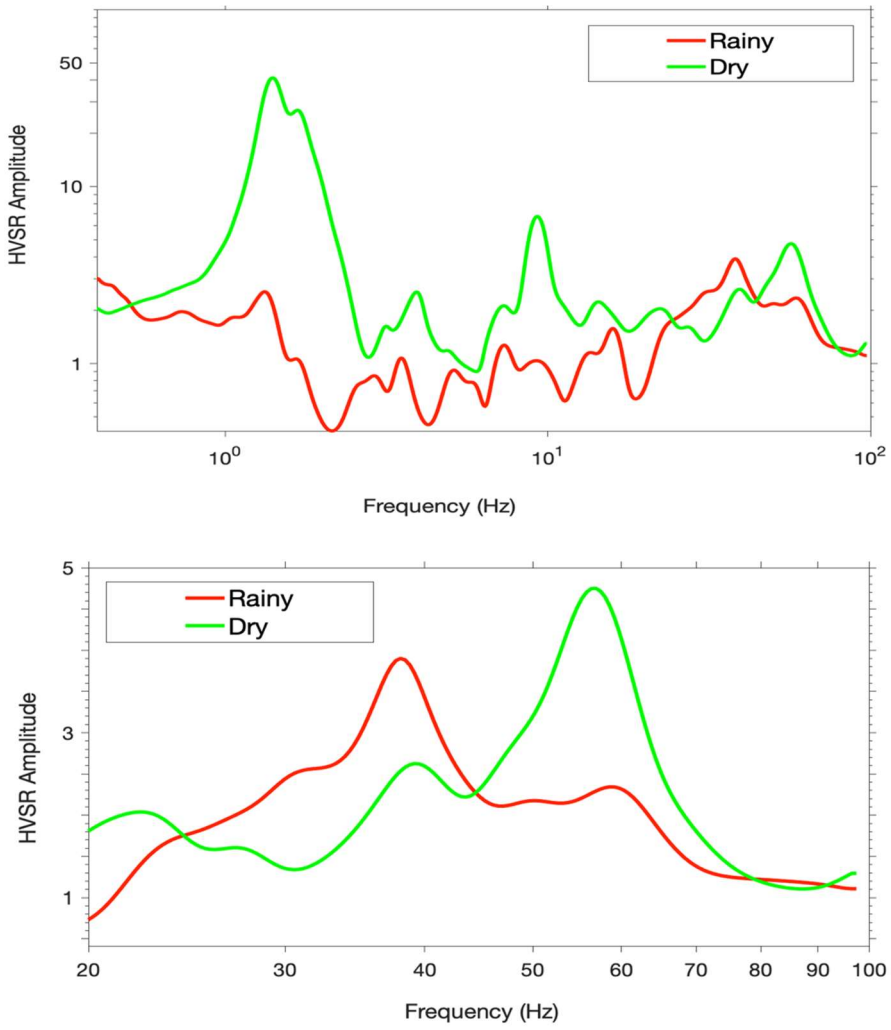

Figure 9 a) Averaged HVSR curves of dry (green curve) and rainy days (red curve). b) Zoom to the higher HVSR peaks found between 20 and 100 Hz.

Furthermore, when observing the frequency changes on a daily basis during the two periods (Figure 11), there is no evidence of daily modulations on any of the three HVSR peaks investigated. Comparison with atmospheric data does not show any evidence of a correlation between the non-periodic HVSR frequency fluctuations observed (Figure 11) and the windspeed and atmospheric pressure series for the two periods studied. We assume that they might have been excited by the river discharge and other related fluvial source mechanisms that can be delineated by detailed seismic studies together with UAV monitoring of the river. According to (Walsh et al. 2020), the frequency signature is a function of turbulence, velocity, viscosity, and density, collectively called a solid-fluid mixture. This relationship has also been

Preprints (www.preprints.org) | NOT PEER-REVIEWED | Posted: 16 November 2022 doi:10.20944/preprints202209.0447.v2

documented elsewhere (Coviello et al. 2019). If the flow velocity increases, the signal will emerge as low frequency while the viscosity damps the high-frequency signatures (Huang et al. 2004). The other factors that affect the frequency spectra by impacting the ground vibrations are the properties of the river bed (geometry, composition, and wetted perimeter) (Kean et al. 2015). There is an increase in the frequency of the seismic signal because of the smoothness and softness of bedrock compared to gravelly or fine sediment composed and dense bedrock, as observed by (Huang et al. 2007). Natural period as a function of changes in Vs can be a possible indicator of loose sediments subjected to detachment in response to EP of the river. The gravel bars in the river floodplain have their natural period and are a source of possible resonance peaks at the HVSR curve. This way, the river bank's compaction and material type can be linked with sediment quantification through natural frequency estimation. These similar features have been delineated based on subsurface stratification achieved by georadar; hence the results are comparable.

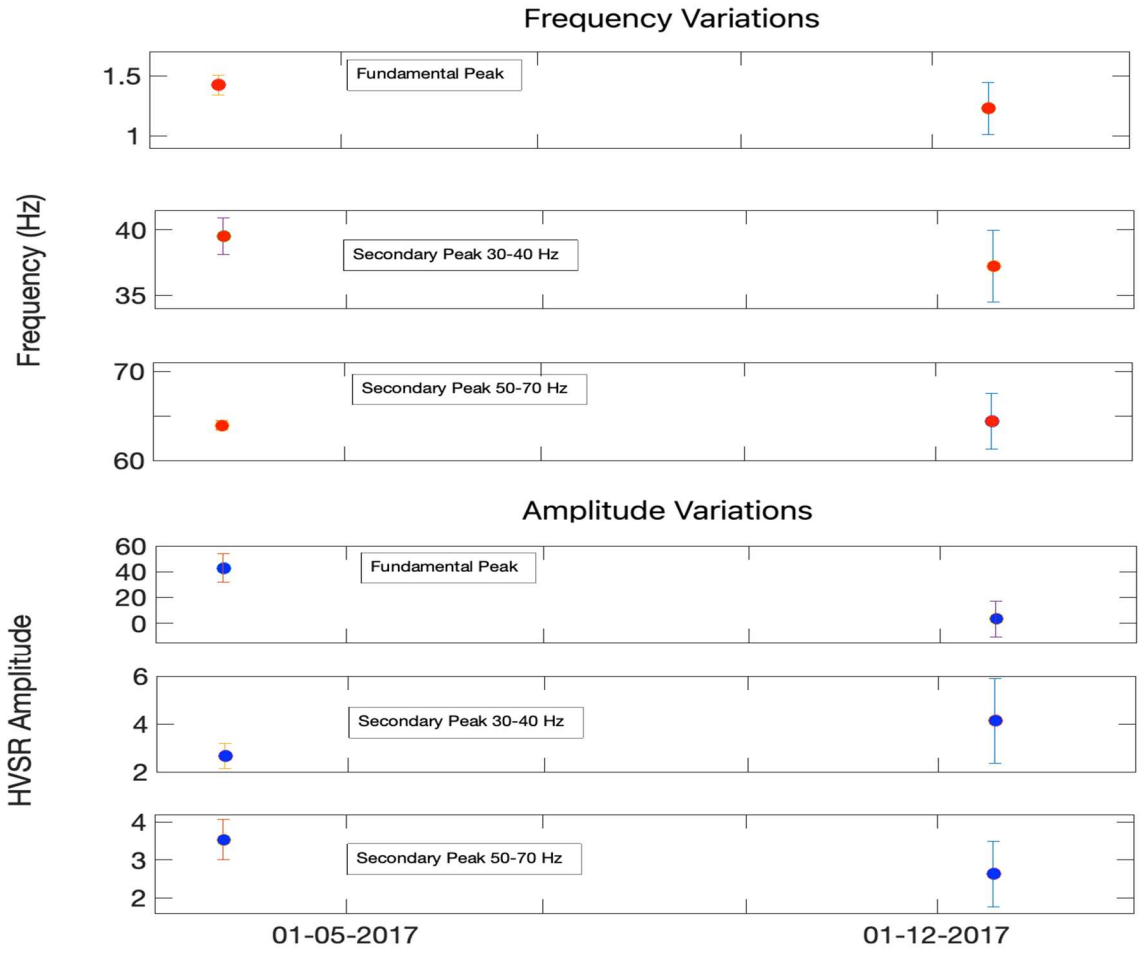

Figure 10. Averaged HVSR variations for the dry (April 2017) and rainy periods (December 2017) measured for the fundamental and secondary peaks observed. Error bars show the standard deviation.

Figure 11. HVSR amplitude variations sampled hourly for the a) fundamental and higher HVSR peaks at b) 40 Hz and c) 60 Hz for dry (April 2017) and rainy periods (December 2017).

Preprints (www.preprints.org) | NOT PEER-REVIEWED | Posted: 16 November 2022 doi:10.20944/preprints202209.0447.v2

Figure 12. HVSR frequency variations sampled hourly for the a) fundamental and higher HVSR peaks at b) 40 Hz and c) 60 Hz for dry (April 2017) and rainy periods (December 2017).

3.2 Site characterization by GPR

The GPR coherence attribute provides additional evidence on the subsurface characterization of the stream bed in the floodplain. Boulders, pebbles, and compacted soil have higher coherence values and more reflection interfaces, whereas unconsolidated or erodible soil shows lower coherence values and lower reflection interfaces. These material interferences are also delineated using coherence attributes where a clear boundary between the valid and invalid signals is found, which is associated with the bedrock interface. We used the "manual pick" mode of ReflexW software to plot the boundary according to the information reflected by the coherence attributes (see Figure 13). GPR images are naturally divided into valid and invalid signal regions, and the green line is also shown in other GPR images (Figures 13, 14 & 15). In the valid region of the GPR data profile, the reflection wave signals are dominated, while the invalid region, doesn't show reflection and can't be used to interpret geological units. There are two possible explanations for marking the depth boundary: electrical conductivity, the signal transmitted by GPR decayed to zero on reaching the depth marked by the green line in Figure 13. Another reason could be the presence of a compacted bedrock interface without a reflector (no reflection wave goes back), and GPR can only record random noise signals.

Figure 13. GPR coherence attribute a) profile 046 and b) profile 002. The green line is interpreted as the boundary between valid and invalid signals.

Contrasted with the traditional GPR image, where the boundary is considered the termination position or bottom of a dense, strong amplitude region (Al-fares et al. 2002), the coherence attribute can reduce the ambiguity and subjectivity of the boundary interpretation. The black dashed line in Figure 14 marks the different parts of the probable boundary interpreted by the traditional method, with the boundary (green line) interpreted using the coherence attribute. The traditional interpretation method can probably ignore the weak amplitude signals that contain effective reflection signals, such as the area between the black dashed line and the solid green line in Figure 14. The coherence attribute wipes off the amplitude information of signals and only reflects the signal waveforms, which reduces the ambiguities in the boundary interpretation.

We acquired the GPR data in the dry season, so the soil water content and conductivity are lower compared to the rainy season. In this way, the deeper penetration of GPR signals in the soil can be achieved as well as the invalid signal region corresponds to the highly compacted bedrock leading to a reduction in the emergence of the reflection interface. In the valid region, a low coherence value indicates the change in subsurface media or structure, such as the presence of rock fragments, pebbles, soil voids, small faults or other related discontinuities. The region corresponding to the high coherence value (white color) presents a higher degree of compaction relative to the corresponding low coherence value (black color) parts in the valid region. Therefore, we consider this position reflected by the black low coherence value in the valid region as the susceptible points to erosion. For instance, soil voids or discontinuity can provide permeable paths where rainwater can infiltrate into the subsurface and may cause instability by building pore water pressure (Hussain et al. 2020b).

Figure 14. Traditional GPR images a) profile 002and b) profile 046. The solid green and dashed black lines are interpreted by the traditional method and coherence attribute, respectively.

Preprints (www.preprints.org) | NOT PEER-REVIEWED | Posted: 16 November 2022 doi:10.20944/preprints202209.0447.v2

The average energy attribute can be used to delineate the presence and geometry of buried pebbles or boulders to the fact that the interface of rock and soil can reflect high energy waves with significant differences in electrical properties among them. Therefore, the places of high energy value may correspond to the positions of subsurface boulders. Information about their sizes can be inferred from the dimensions of the purple color regions on the energy attribute image (Figure 15).

Figure 15. GPR average energy attribute a) profile 002 and b) profile 046. The green line is the boundary of the valid and invalid signal regions. The purple color is high in average energy value, while white and gray are lower values. The blue circles marked out some possible boulders underground.

The traditional GPR images in Figure 15 contain purple and blue colors to display the strong positive and negative signals to observe the stratigraphy featured. Figure 16 clearly reflects that the subsurface layers generally are the distribution characteristics of approximately horizontal deposition. Some tilted deposit layers are also evident in the images, especially in Figure 16a. Only the valid signal region can be applied for the stratigraphy interpretation in the average amplitude attribute (Figure 16). The average amplitude attribute can be more convenient and visual for layer depth interpretation.

Figure 16. GPR amplitude attribute a) profile 002 and b) profile 046. The green line is the boundary of the valid and invalid signal regions. Purple is high value, and white and gray are low value.

ANb signatures of the streams on flooding days, along with erosion-prone conditions (colluvium and boulders) of stream beds inferred from georadar attribute analysis, can help in the estimation of stream EPs that promote reverie landslides and soil losses in the fluvial valleys. The higher EP, together with the presence of mechanically weak lithologies, lead to geological hazards (landslide and soil losses). As ambient noise level is sensitive to the changes in flood and sediment loads of the river, this can help in the quantification of force exerted by the flood on critical infrastructures (e.g., bridges, flood-resistant structures and many others) and hence assist in the estimation of their resilience and can be used as a precursor for the possible damage evaluations that river may cause during floods. The future climate change scenarios can also be predicted in this way. Such understanding may help minimize the damages and soil losses, as an important step in retaining agriculture in the Cerrado region of Brazil.

4 Conclusions

This study presents seismic monitoring and analysis of the river sediment carrying capacity in the *Ribeirão Contagem* watershed (of the Federal district of Brazil) on rainy and dry days. The GPR-based local site conditions and their possible impacts on the erosion and sediment load of the river are discussed. The ambient noise wavefields during dry and rainy days are measured and compared. This comparison was conducted by applying spectral analysis of the ambient noise (recorded two times), including power spectral density estimation, time-frequency analysis by spectrogram, and possible quantification effects on the site response by HVSR curves. Additionally, the GPR attributes are studied for the delineation of erosion-prone sites as a major source of geohazard and sediment quality in the river of the fluvial valley. Based on the findings, we may conclude the followings:

i) Ambient noise-based analysis showed variations in the PSD on rainy and dry days. An apparent change in the spectrogram of rainy days was identified, attributed to rainfall and river dynamics. PSD vs meteorological agent (rainfall and wind speed) plots showed changes in PSD during rainy days.

ii) Based on the spectrograms of the rainy days (the signals and their characteristics), it can be suggested that one of the signals dominantly results from bedload transport and the other two from fluid transport processes.

iii) The HVSR plots showed an increase in amplitude starting from 10 Hz. During rainy days, a shift to low frequency and a semi-diurnal modulation on the higher peaks are observed.

iv) Ambient noise RMS plots evidently showed variations in displacement during daytime. The correspondence between wind speed and seismic energy CPA demonstrates that both phenomena are somehow correlated.
Based on the variations and emergence of new typologies on different frequency bands, we assume that they might have been excited by the river discharge and other related fluvial source mechanisms that can be delineated by detailed seismic studies together with UAV monitoring of the river.

v) GPR average amplitude attribute profiles showed the detailed riverbank and floodplain stratigraphy, including depth and topography of bedrock. The presence of boulders of various sizes is identified by the GPR energy attributes. In contrast, the coherence attribute helped in evaluating the degree of compaction and a possible indication of the region as susceptible to erosion (weak spots). The invalid region corresponds to a high degree of compaction area in the subsurface because a little reflection surface can reflect waves, and GPR can only record random noise.

From our seismic noise analysis performed in Brasilia, it is evident that a seismometer can be an efficient tool to characterize the seismic signature of the river (at high frequency) to quantify better the river activity, particularly the bed load transport during floods. In addition, the presence of fluvial lithologies (boulder and colluvial sediments) and the slope steepness, characteristics of fluvial valleys such as Ribeirão Contagem, make it vulnerable to natural hazards (landslides and erosion). This is closely related to rainfall and lithologies, motivating a better understanding of the phenomena to help decipher such destructive environmental processes. This study is a preliminary step in integrating stream bed conditions and flood levels using remote, cheaper and non-invasive geophysical applications. The present study will allow further field investigation to improve the estimation of sediment transport during flood events by deploying seismometers along rivers in fluvial valleys.

Acknowledgment:

Statements and Declarations:

There is no competing interest among the authors.

Data Availability: Data are available by emailing the corresponding author.

References

Al-fares W, Bakalowicz M, Guérin R, Dukhan M (2002) Analysis of the karst aquifer structure of the Lamalou area (Hérault, France) with ground penetrating radar. J Appl Geophys 51:97–106. https://doi.org/10.1016/S0926-9851(02)00215-X

Albarello D, Lunedei E (2013) Combining horizontal ambient vibration components for H/V spectral ratio estimates. Geophys J Int 194:. https://doi.org/10.1093/gji/ggt130

Amorese D, Grasso J-R, Garambois S, Font M (2018) Change-point analysis of geophysical time-series: application to landslide displacement rate (Séchilienne rock avalanche, France). Geophys J Int 213:1231–1243. https://doi.org/10.1093/gji/ggy060

Anthony RE, Aster RC, Ryan S, et al (2018) Measuring Mountain River Discharge Using Seismographs Emplaced Within the Hyporheic Zone. J Geophys Res Earth Surf 123:210–228. https://doi.org/10.1002/2017JF004295

Araujo HA, Cooper AB, Hassan MA, Venditti J (2012) Estimating suspended sediment concentrations in areas with limited hydrological data using a mixed-effects model. Hydrol Process 26:3678–3688. https://doi.org/10.1002/hyp.8462

Arcone SA, Lawson DE, Delaney AJ, et al (1998) Ground-penetrating radar reflection profiling of groundwater and bedrock in an area of discontinuous permafrost. Geophysics 63:1573–1584. https://doi.org/10.1190/1.1444454

Bahorich M, Farmer S (1995) The coherence cube. Lead Edge

Bakker M, Gimbert F, Geay T, et al (2020) Field Application and Validation of a Seismic Bedload Transport Model. J Geophys Res Earth Surf 125:e2019JF005416. https://doi.org/10.1029/2019JF005416

Barrière J, Oth A, Hostache R, Krein A (2015) Bed load transport monitoring using seismic observations in a low-gradient rural gravel bed stream. Geophys Res Lett 42:2294–2301. https://doi.org/10.1002/2015GL063630

Bartholomaus TC, Amundson JM, Walter JI, et al (2015) Subglacial discharge at tidewater glaciers revealed by seismic tremor. Geophys Res Lett 42:6391–6398. https://doi.org/10.1002/2015GL064590

Braga LM, Caldeira D, da Silva Nunes JG, et al (2018) Geomorphological description and erosive-depositional dynamics of hillslopes on Ribeirão Contagen Fluvial Valley-DF, Brazil. Anu do Inst Geociencias 41:51–65. https://doi.org/10.11137/2018_2_51_65

Burtin A, Bollinger L, Vergne J, et al (2008) Spectral analysis of seismic noise induced by rivers: A new tool to monitor spatiotemporal changes in stream hydrodynamics. J Geophys Res 113:B05301. https://doi.org/10.1029/2007JB005034

Burtin A, Cattin R, Bollinger L, et al (2011) Towards the hydrologic and bed load monitoring from high-frequency seismic noise in a braided river: The “torrent de St Pierre”, French Alps. J Hydrol 408:43–53. https://doi.org/10.1016/j.jhydrol.2011.07.014

Chalikakis K, Plagnes V, Guerin R, et al (2011) Contribution of geophysical methods to karst-system exploration: An overview. Hydrogeol J 19:1169–1180. https://doi.org/10.1007/s10040-011-0746-x

Chao WA, Wu YM, Zhao L, et al (2015) Seismologically determined bedload flux during the typhoon season. Sci Rep 5:1–8. https://doi.org/10.1038/srep08261

 doi:10.20944/preprints202209.0447.v2

Chmiel M, Godano M, Piantini M, et al (2022) Brief communication: Seismological analysis of flood dynamics and hydrologically triggered earthquake swarms associated with Storm Alex. Nat Hazards Earth Syst Sci 22:1541–1558. https://doi.org/10.5194/nhess-22-1541-2022

Colombero C, Jongmans D, Fiolleau S, et al (2021) Seismic Noise Parameters as Indicators of Reversible Modifications in Slope Stability: A Review. Surv. Geophys. 42

Coviello V, Arattano M, Comiti F, et al (2019) Seismic Characterization of Debris Flows: Insights into Energy Radiation and Implications for Warning. J Geophys Res Earth Surf 124:1440–1463. https://doi.org/10.1029/2018JF004683

Cunha ER da, Santos CAG, Silva RM da, et al (2022) Assessment of current and future land use/cover changes in soil erosion in the Rio da Prata basin (Brazil). Sci Total Environ 818:151811. https://doi.org/10.1016/j.scitotenv.2021.151811

da Silva Nunes JG, Uagoda R, Caldeira D, et al (2019) Application of GPR for the differentiation of alluvial and colluvial materials, based on direct observation in Contagem Valley – Distrito Federal (Brasil). Rev Bras Geomorfol 20:217–238. https://doi.org/10.20502/rbg.v20i2.1382

David MB, Drinkwater LE, McIsaac GF (2010) Sources of Nitrate Yields in the Mississippi River Basin. J Environ Qual 39:1657–1667. https://doi.org/10.2134/jeq2010.0115

Díaz J, Ruíz M, Crescentini L, et al (2014) Seismic monitoring of an Alpine mountain river. J Geophys Res Solid Earth 119:3276–3289. https://doi.org/10.1002/2014JB010955

Fabregat I, Gutiérrez F, Roqué C, et al (2019) Subsidence mechanisms and sedimentation in alluvial sinkholes inferred from trenching and ground penetrating radar (GPR). Implications for subsidence and flooding hazard assessment. Quat Int 525:1–15. https://doi.org/10.1016/j.quaint.2019.09.008

Falanga M, Cusano P, De Lauro E, Petrosino S (2021) Picking up the hydrothermal whisper at Ischia Island in the Covid-19 lockdown quiet. Sci Rep 11:. https://doi.org/10.1038/s41598-021-88266-9

Ferreira, R., Uagoda R (2015) Morphometric study of controls to erosional features and identification of areas susceptible to mass movement hazards in the contagem watershed, Distrito Federal. Rev Espaço e Geogr 18:187:216

Fonseca MRS, Uagoda R, Chaves HML (2022) Rates, factors, and tolerances of water erosion in the Cerrado biome (Brazil): A meta-analysis of runoff plot data. Earth Surf Process Landforms 47:582–595. https://doi.org/10.1002/esp.5273

Gabet EJ, Burbank DW, Pratt-Sitaula B, et al (2008) Modern erosion rates in the High Himalayas of Nepal. Earth Planet Sci Lett 267:482–494. https://doi.org/10.1016/j.epsl.2007.11.059

Gao Q, Wang S, Peng T, et al (2020) Evaluating the structure characteristics of epikarst at a typical peak cluster depression in Guizhou plateau area using ground penetrating radar attributes. Geomorphology 364:. https://doi.org/10.1016/j.geomorph.2019.107015

Gimbert F, Tsai V, Geophysical ML-J of, 2014 undefined (2014) A physical model for seismic noise generation by turbulent flow in rivers. Wiley Online Libr 119:2209–2238. https://doi.org/10.1002/2014JF003201

Giménez R, Casalí J, Grande I, et al Factors controlling sediment export in a small agricultural watershed in Navarre (Spain). Elsevier

Gomes L, Simões SJC, Dalla Nora EL, et al (2019) Agricultural expansion in the Brazilian Cerrado: Increased soil and nutrient losses and decreased agricultural productivity. Land 8:. https://doi.org/10.3390/land8010012

Goodling PJ, Lekic V, Prestegaard K (2018) Seismic signature of turbulence during the 2017 Oroville Dam spillway erosion crisis. Earth Surf Dyn 6:351–367. https://doi.org/10.5194/esurf-6-351-2018

Graf WL, Wohl E, Sinha T, Sabo JL (2010) Sedimentation and sustainability of western American reservoirs. Water Resour Res 46:. https://doi.org/10.1029/2009WR008836

Hamza O, De Vargas T, Boff FE, et al (2020) Geohazard Assessment of Landslides in South Brazil: Case Study. Geotech Geol Eng 38:971–984. https://doi.org/10.1007/s10706-019-01054-1

Huang C-J, Shieh C-L, Yin H-Y (2004) Laboratory study of the underground sound generated by debris flows. J Geophys Res Earth Surf 109:. https://doi.org/10.1029/2003jf000048

Huang C-J, Yin H-Y, Chen C-Y, et al (2007) Ground vibrations produced by rock motions and debris flows. J Geophys Res 112:F02014. https://doi.org/10.1029/2005JF000437

Hussain Y, Cardenas-Soto M, Martino S, et al (2019a) Multiple geophysical techniques for investigation and monitoring of Sobradinho Landslide, Brazil. Sustain 11:. https://doi.org/10.3390/su11236672

Hussain Y, Cardenas-Soto M, Moreira C, et al (2020a) Variation in rayleigh wave ellipticity as a possible indicator of earthflow mobility: A case study of sobradinho landslide compared with pile load testing. Earth Sci Res J 24:141–151. https://doi.org/10.15446/esrj.v24n2.81974

Hussain Y, Cardenas-Soto M, Uagoda R, et al (2019b) Monitoring of Sobradinho landslide (Brasília, Brazil) and a prototype vertical slope by time-lapse interferometry. Brazilian J Geol 49:. https://doi.org/10.1590/2317-4889201920180085

Hussain Y, Hamza O, Cárdenas-Soto M, et al (2020b) Characterization of sobradinho landslide in fluvial valley using masw and ert methods. REM - Int Eng Journal 73:. https://doi.org/10.1590/0370-44672019730109

Hussain Y, Schlögel R, Innocenti A, et al (2022) Review on the Geophysical and UAV-Based Methods Applied to Landslides. Remote Sens 14:4564. https://doi.org/10.3390/rs14184564

Jol H (2008) Ground penetrating radar theory and applications

Kean JW, Coe JA, Coviello V, et al (2015) Estimating rates of debris flow entrainment from ground vibrations. Geophys Res Lett 42:6365–6372. https://doi.org/10.1002/2015GL064811

Lagarde S, Dietze M, Gimbert F, et al (2021) Grain-Size Distribution and Propagation Effects on Seismic Signals Generated by Bedload Transport. Water Resour Res 57:. https://doi.org/10.1029/2020WR028700

Lai VH, Tsai VC, Lamb MP, et al (2018) The Seismic Signature of Debris Flows: Flow Mechanics and Early Warning at Montecito, California. Geophys Res Lett 45:5528–5535. https://doi.org/10.1029/2018GL077683

Lawler DM (1993) The measurement of river bank erosion and lateral channel change: A review. Earth Surf Process Landforms 18:777–821. https://doi.org/10.1002/esp.3290180905

Lecocq T, Hicks SP, van Noten K, et al (2020) Global quieting of high-frequency seismic noise due to COVID-19 pandemic lockdown measures. Science (80-) 369:1338–1343. https://doi.org/10.1126/science.abd2438

Lykou R, Tsaklidis G, Papadimitriou E (2020) Change point analysis on the Corinth Gulf (Greece) seismicity. Phys A Stat Mech its Appl 541:. https://doi.org/10.1016/j.physa.2019.123630

Maciel STR, Rocha MP, Schimmel M (2021) Urban seismic monitoring in Brasilia, Brazil. PLoS One 16:. https://doi.org/10.1371/journal.pone.0253610

Marchetti E, Walter F, Barfucci G, et al (2019) Infrasound Array Analysis of Debris Flow Activity and Implication for Early Warning. J Geophys Res Earth Surf 124:567–587. https://doi.org/10.1029/2018JF004785

Nakamura Y (1989) Method for dynamic characteristics estimation of subsurface using microtremor on the ground surface. Q Rep RTRI (railw Tech Res Institute) 30:

Oeurng C, Sauvage S, Sánchez-Pérez JM (2010) Dynamics of suspended sediment transport and yield in a large agricultural catchment, southwest France. Earth Surf Process Landforms 35:1289–1301. https://doi.org/10.1002/esp.1971

P.C S, Sawazaki K (2021) River discharge prediction for ungauged mountainous river basins during heavy rain events based on seismic noise data. Prog Earth Planet Sci 8:. https://doi.org/10.1186/s40645-021-00448-1

Pandey AP, Singh AP, Bansal BK, et al (2020) Appraisal of seismic noise scenario at national seismological network of India in COVID-19 lockdown situation. Geomatics, Nat Hazards Risk 11:2095–2122. https://doi.org/10.1080/19475705.2020.1830187

Piantini M, Gimbert F, Bellot H, Recking A (2021) Triggering and propagation of exogenous sediment pulses in mountain channels: Insights from flume experiments with seismic monitoring. Earth Surf Dyn 9:1423–1439. https://doi.org/10.5194/esurf-9-1423-2021

Polvi LE, Dietze M, Lotsari E, et al (2020) Seismic Monitoring of a Subarctic River: Seasonal Variations in Hydraulics, Sediment Transport, and Ice Dynamics. Wiley Online Libr 125:. https://doi.org/10.1029/2019JF005333

Rindraharisaona EJ, Réchou A, Fontaine FR, et al (2022) Seismic Signature of Rain and Wind Inferred From Seismic Data. Earth Sp Sci 9:295. https://doi.org/10.1029/2022EA002328

Roth DL, Brodsky EE, Finnegan NJ, et al (2016) Bed load sediment transport inferred from seismic signals near a river. Wiley Online Libr 121:725–747. https://doi.org/10.1002/2015JF003782

Saccorotti G, Piccinini D, Cauchie L, Fiori I (2011) Seismic noise by Wind Farms: A case study from the Virgo Gravitational Wave Observatory, Italy. Bull Seismol Soc Am 101:568–578. https://doi.org/10.1785/0120100203

Sánchez-Pastor P, Obermann A, Schimmel M (2018) Detecting and Locating Precursory Signals During the 2011 El Hierro, Canary Islands, Submarine Eruption. Geophys Res Lett 45:10,288-10,297. https://doi.org/10.1029/2018GL079550

Sánchez-Sesma FJ, Rodríguez M, Iturrarán-Viveros U, et al (2011) A theory for microtremor H/V spectral ratio: Application for a layered medium. Geophys J Int 186:. https://doi.org/10.1111/j.1365-246X.2011.05064.x

Schimmel A, Hübl J, McArdell BW, Walter F (2018) Automatic identification of alpine mass movements by a combination of seismic and infrasound sensors. Sensors (Switzerland) 18:. https://doi.org/10.3390/s18051658

Schmandt B, Aster RC, Scherler D, et al (2013) Multiple fluvial processes detected by riverside seismic and infrasound monitoring of a controlled flood in the Grand Canyon. Geophys Res Lett 40:4858–4863. https://doi.org/10.1002/grl.50953

Schneider JM, Turowski JM, Rickenmann D, et al (2014) Scaling relationships between bed load volumes, transport distances, and stream power in steep mountain channels. J Geophys Res Earth Surf 119:. https://doi.org/10.1002/2013JF002874

Seivane H, García-Jerez A, Navarro M, et al (2022) On the use of the microtremor HVSR for tracking velocity changes: a case study in Campo de Dalías basin (SE Spain). Geophys J Int 230:542–564. https://doi.org/10.1093/gji/ggac064

SESAME (2004) Guidelines for The Implementation of The H/V Spectral Ratio Technique on Ambient Vibrations-Measurements, Processing and Interpretations, SESAME European Research Project. SESAME Site Eff Assess using Ambient Excit 1–62

Singh AP, Kumar MR, Pandey A, Roy KS (2019) Investigation of spatial and temporal variability of site response in the Arunachal Himalaya using ambient seismic noise and earthquake waveforms. Near Surf Geophys 17:427–445. https://doi.org/10.1002/nsg.12053

Smith K, Tape C (2019) Seismic Noise in Central Alaska and Influences From Rivers, Wind, and Sedimentary Basins. J Geophys Res Solid Earth 124:11678–11704. https://doi.org/10.1029/2019JB017695

 doi:10.20944/preprints202209.0447.v2

Somos-Valenzuela MA, Mckinney DC, Byers AC, et al (2015) Assessing downstream flood impacts due to a potential GLOF from Imja Tsho in Nepal. Hydrol Earth Syst Sci 19:1401–1412. https://doi.org/10.5194/hess-19-1401-2015

Stevens NT, James SR (2022) Capturing the Changing Cryosphere with Seismic Horizontal-Vertical Spectral Ratios. FastTIMES 26:

Szuch RP, White JG, Vepraskas MJ, Doolittle JA (2006) Application of ground penetrating radar to aid restoration planning for a drained carolina BAY. Wetlands 26:205–216

Truong C, Oudre L, Vayatis N (2020) Selective review of offline change point detection methods. Signal Processing 167

Tsai VC, Minchew B, Lamb MP, Ampuero J-P (2012) A physical model for seismic noise generation from sediment transport in rivers. Res Lett 39:2404. https://doi.org/10.1029/2011GL050255

Turowski JM, Badoux A, Rickenmann D (2011) Start and end of bedload transport in gravel-bed streams. Geophys Res Lett 38:. https://doi.org/10.1029/2010GL046558

Walsh B, Coviello V, Capra L, et al (2020) Insights Into the Internal Dynamics of Natural Lahars From Analysis of 3-Component Broadband Seismic Signals at Volcán de Colima, Mexico. Front Earth Sci 8:. https://doi.org/10.3389/feart.2020.542116

Wang P, Hu Z, Zhao Y, Li X (2016) Experimental study of soil compaction effects on GPR signals. J Appl Geophys 126:128–137. https://doi.org/10.1016/j.jappgeo.2016.01.019

Weihermüller L, Huisman JA, Lambot S, et al (2007) Mapping the spatial variation of soil water content at the field scale with different ground penetrating radar techniques. J Hydrol 340:205–216. https://doi.org/10.1016/j.jhydrol.2007.04.013

Wenner M, Walter F, McArdell B, Farinotti D (2019) Deciphering debris-flow seismograms at Illgraben, Switzerland. In: Debris-Flow Hazards Mitigation: Mechanics, Monitoring, Modeling, and Assessment - Proceedings of the 7th International Conference on Debris-Flow Hazards Mitigation. pp 222–229

Wilcock PR, Crowe JC (2003) Surface-based Transport Model for Mixed-Size Sediment. J Hydraul Eng 129:. https://doi.org/10.1061/(asce)0733-9429(2003)129:2(120)

Young RA, Deng Z, Marfurt KJ, Nissen SE (1997) 3-D dip filtering and coherence applied to GPR data: A study. Lead Edge 16:921. https://doi.org/10.1190/1.1437699

Zhang J, Zhou L, Huang D (2022) Development of rill erosion on bare sloping farmland under natural rainfall conditions. Environ Earth Sci 81:. https://doi.org/10.1007/s12665-022-10383-z